

PRELIMINARY EVALUATION OF EARTH-MOON LIBRATION POINT ORBIT NAVIGATION WITH POST-PROCESSED ARTEMIS DATA

Jason M. Leonard⁽¹⁾, Bradley W. Cheetham⁽²⁾, and George H. Born⁽³⁾

⁽¹⁾Colorado Center for Astrodynamics Research, Aerospace Engineering Sciences, University of Colorado Boulder, 431 UCB Boulder CO 80309, 303-735-2921, jason.leonard@colorado.edu

⁽²⁾Colorado Center for Astrodynamics Research, Aerospace Engineering Sciences, University of Colorado Boulder, 431 UCB Boulder CO 80309, 303-492-1142, bradley.cheetham@colorado.edu

⁽³⁾Colorado Center for Astrodynamics Research, Aerospace Engineering Sciences, University of Colorado Boulder, 431 UCB Boulder CO 80309, 303-492-8638, georgeb@colorado.edu

Abstract:

The existence of raw operational data from the first mission to maintain libration point orbits in the Earth-Moon three-body regime provides a rare opportunity to research navigation approaches to better prepare mission designers and operators for future missions. Leveraging this raw data, a navigation filter has been assembled and demonstrated. This capability has been further leveraged to evaluate the precision of solutions using multiple overlap analyses spanning several months of satellite data. Long arcs of data were processed and detailed solar coefficients were estimated to establish consistent spacecraft parameters. This increased accuracy in the spacecraft solar coefficients combined with an ability to process data sequentially, enabled the estimation of station-keeping maneuvers and subsequent comparison with intended maneuver designs.

Keywords: Navigation, Earth-Moon Libration Point Orbits, Operations, Estimation, Filtering

1. Introduction

Orbits of spacecraft in the Earth-Moon three-body regime provide particular benefits for a variety of science and exploration missions. The focus of ongoing work which will be discussed in this paper is to better understand the dynamic environment and operational constraints of spacecraft in this orbital regime. The specific focus of this work are libration point orbits (LPOs) about the Earth-Moon co-linear L1 and L2 points. These orbits are unstable and thus require frequent station-keeping maneuvers to remain in the region. These station-keeping maneuvers are a primary driver of operational utility and previous studies have estimated the total cost of station-keeping to vary from approximately 1-4 m/s/yr to more than 50 m/s/yr. The former figure is based on orbit determination accuracy better than 10 meters [1] and the latter is based on dynamics including modeling and maneuver errors [2]. This paper will discuss work that seeks to improve the navigation solutions of missions in Earth-Moon LPOs. Improved navigation solutions are expected to have a direct impact on both the total delta-v required for these missions as well as the tracking and staffing requirements during orbital operations.

To obtain these operational improvements, raw tracking data from the **A**cceleration, **R**econnection, **T**urbulence and **E**lectrodynamics of the **M**oons **I**nteraction with the **S**un (ARTEMIS) mission is used to evaluate sources of navigational errors. The ARTEMIS mission is unique in that it was the first mission to ever maintain LPOs in the Earth-Moon system. The ARTEMIS mission utilized

two spacecraft from the **Time History of Events and Macroscale Interactions during Substorms (THEMIS)** mission constellation and employed a highly efficient orbital transfer to relocate these spacecraft from high Earth orbits to the Moon [3, 4, 5]. These two spacecraft are operationally referred to as P1 and P2. This naming convention will be maintained in this paper. The spacecraft designated P1 maintained LPO from approximately August 25th 2010 until June 6th 2011 while P2 maintained LPO from approximately October 20th 2010 until June 10th 2011. The station-keeping budget for ARTEMIS was approximately 15 m/s for each spacecraft during the planned ~6 month L1/L2 orbit maintenance portion of the mission. The magnitude of these station keeping maneuvers is driven primarily by the accuracy of navigation solutions and maneuver execution errors.

The primary motivation of this and future work is to evaluate the raw data from the ARTEMIS mission to develop a body of knowledge relevant to navigating spacecraft in Earth-Moon LPOs. This body of knowledge seeks to improve the operational efficacy of future missions planning to utilize this environment for space science and exploration. Previous work by the authors established a baseline for this study using simulated data [6]. Current work is leveraging raw data from the ARTEMIS mission. The work presented here is based on evaluating data from the P2 spacecraft.

This paper specifically will review the processes used to evaluate the raw operational data, discuss results of processing the data in between maneuvers, review solutions generated from processing data over maneuvers, and demonstrate preliminary results for increased fidelity estimates of solar coefficients. These results will be evaluated using overlap comparisons to draw conclusions on the precision of orbit solutions.

2. Technical Overview

Previously, simulated data was evaluated to better understand the navigation environment in LPO regions. This simulated data used spacecraft parameters and mission information meant to relate to the ARTEMIS operational mission. Upon completion of this preliminary work using simulated data, the research moved to look at what information could be derived from the raw operational data during the LPO mission phase.

Processing raw tracking data required significant new development work to establish the functionality in software tools at the Colorado Center for Astrodynamics Research capable of generating and evaluating navigation solutions. The following sub-sections will provide a high level overview of select development activities.

2.1. MONTE

The **Mission analysis and Operational Navigation Toolkit Environment (MONTE)** software was developed at NASA's Jet Propulsion Laboratory (JPL) to replace legacy navigation software DP-TRAJ/ODP [7]. MONTE was developed to help support trajectory and navigation analysis and design for spacecraft missions. The MONTE software provides a set of functions that enable the design, estimation, and control of spacecraft trajectories. MONTE relies heavily on object-oriented programming, thus allowing a user to construct object instances with callable functions.

The general form of MONTE’s discrete-time kalman filter can be found in Bierman [8]. The estimated state vector can be separated into three categories: estimated parameters, stochastic parameters, and consider parameters. The estimated parameters include both dynamic and bias parameters whose covariance can be affected by the state transition matrix time updates but are not affected by any process noise or stochastics directly. Stochastic parameters are those parameters that can change over a time interval due to a discrete noise process. These discrete-time process noise stochastic parameters are applied at regular intervals, known as batches. Consider parameters have uncertainties that are fed into the estimation process but their values are not estimated [9].

2.2. Tracking Data and File Formats

Observation data for the ARTEMIS mission is primarily S-band radiometric tracking data from several ground stations. The ARTEMIS tracking data comes from three primary ground-based tracking networks which include the Deep Space Network (DSN), the Universal Space Network (USN) and the Berkeley Ground Station (BGS). DSN tracking data was supplied in TRK-2-34 format and then converted to a Universal Tracking Data Format (UTDF) format with both Doppler and Range measurements. The Doppler measurements were compressed to 60 second count data. BGS supplied Doppler tracking in UTDF format with primarily 10 second count data and some high-density data with 0.1 second count intervals. BGS does supply Range measurements. However, due to the link margin at BGS, Range data is generally not reliable. The USN tracking data was also in UTDF format with both Range and Doppler measurements with a count time of 5 seconds. This data was similarly compressed to 60 second count data and for the purposes of the solutions in this paper was not included in the filter runs.

2.3. Overlap Analysis

Comparing outputs from the navigation filter and generating reliable estimates for uncertainty and quality of solutions is a challenge with operational data. To evaluate the precision, or consistency, of orbit solutions generated with the raw tracking data for this work, overlap analyses were conducted [10, 11]. These overlap analyses were able to provide insight into the solutions being generated and provide a metric for evaluating the performance of the navigation filter.

The various approaches to processing the data necessitated two overlap strategies. A short-arc overlap was conducted to evaluate the navigation solutions between maneuvers. These solutions begin immediately after a station-keeping maneuver and end immediately before the next station-keeping maneuver. Once the ability to filter over and estimate maneuvers was demonstrated, a subsequent overlap approach which considered orbit solutions spanning over maneuvers was

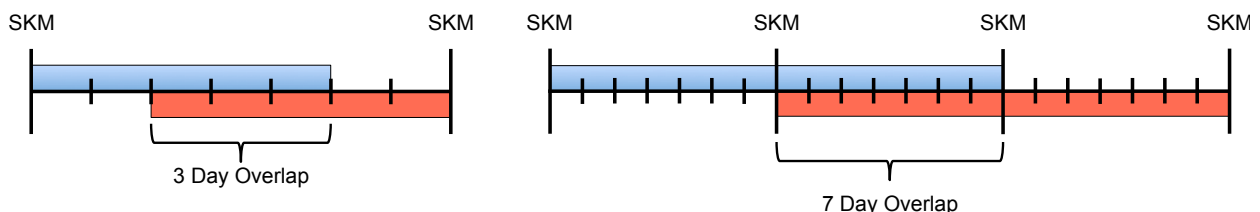


Figure 1: Schematic of 3-day and 7-day Overlaps

employed. In this analysis, these overlap studies are considered long-arc overlaps and generally consider periods spanning two station-keeping maneuvers. Fig. 1 gives a simple schematic of the overlap strategy used in this paper.

2.4. Orbit Determination Set-up

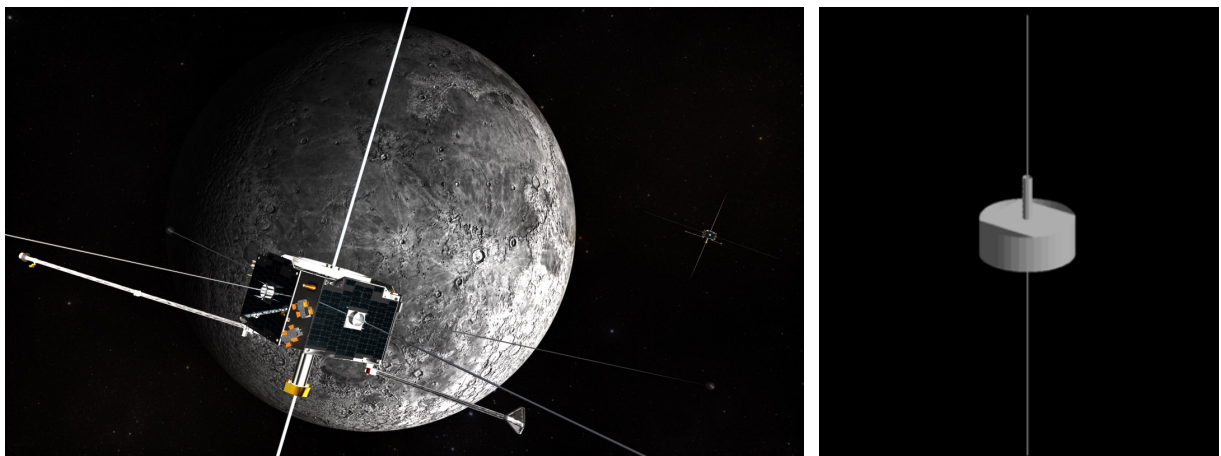
The orbit determination procedure used to process the ARTEMIS tracking data and generate reliable solution estimates is an intricate process. There are several pre-processing stages that must be completed before any estimation can take place. The first pre-processing step was the conversion of ARTEMIS tracking data from UTDF format to a format that MONTE can read. Tracking data for the DSN, BGS, and USN from 2010 and 2011 were converted to a MONTE readable measurement format for both Two-way ranging and Two-way Doppler measurements. Due to run-time concerns and the dense Doppler tracking, all Doppler measurements were then compressed to a 60 second count time. This compression drastically reduced the noise level of the BGS Doppler measurements.

A major source of error for radiometric ground measurements is due to the propagation delay of a radio signal caused by the troposphere and ionosphere. The accuracy of radiometric ranging is greatly affected by the residual errors in modeling signal propagation delay through the troposphere and stratosphere. The main modeling method used in this work to mitigate the effects of the tropospheric delay rely on measurements of the zenith dry and wet delays at the ground station. These zenith delays are then mapped using the Niell mapping function [12]. A seasonal model for each ground station complex is obtained from monthly averages of zenith delay [13]. A 10th order polynomial is then fit to 3 days worth of zenith delays that deviate from the seasonal model for the duration of the mission. The dispersive effects of the ionosphere on radio signal propagation are generally accounted for by a linear combination of observations with multiple frequencies. However, standard interplanetary navigation utilizes a single frequency that must be corrected as much as possible for the total ionospheric delay. The first order ionospheric delay terms contribute to 99.9% of the total ionospheric delay [14]. The first order ionospheric delay depends only on the Slant Total Electron Content (STEC). For this analysis, global Vertical Total Electron Content (VTEC) maps were obtained from the International GNSS Service (IGS) that were then interpolated spatially and through time [15]. A thin shell spherical layer mapping model is then used to convert the interpolated VTEC values into the necessary STEC. An ionospheric delay is then calculated for each ground station based on the ground stations position and the position of the spacecraft. The total ionospheric delay during an observation pass is fit to a 10th order polynomial and applied to the observations during the filtering process.

The next part of the OD procedure was the determination and initialization of dynamic models to use in the trajectory propagation and estimation. The main perturbing dynamics that are included in this analysis are that of gravity, solar radiation pressure, and random acceleration perturbations. The JPL planetary ephemeris DE421 is used for the positions of the celestial bodies [16]. The three main celestial bodies perturbing the ARTMEIS-P2 trajectory are that of the Earth, Moon, and Sun. The Earth was considered to be the main perturbing body with third-body gravitational perturbations evaluated from the Moon, Sun, and remaining planets. The Earth's non-spherical gravity was modeled using GGM02C with a 16x16 spherical harmonic representation [17]. The Moon's non-spherical gravity was modeled using the GRAIL derived GL0660B model with a 16x16

spherical harmonic representation [18]. The Earth’s body-fixed orientation is represented by ITRF standards with Earth Orientation Parameter (EOP) updates. The Moon’s body-fixed orientation is represented by the lunar librations present in the DE421 ephemeris.

Solar radiation pressure is included with a solar constant of 1366 W/m^2 at 1 AU. The spacecraft is modeled with a cylinder as the spacecraft bus, a one-sided top and bottom plate, a cylindrical antenna boom, and a cylindrical axial boom. The actual ARTEMIS spacecraft has a square bus with rectangular side plates as seen in Fig. 2(a). The shape model used in this analysis can be seen in Fig. 2(b). A cylindrical bus shape was chosen for this analysis since the ARTEMIS spacecraft has a spin rate of roughly 20 RPM throughout the mission. It was assumed that this spin rate with rectangular plates would average out the SRP effects similar to that of a cylinder with the same cross-sectional area.



(a) Real

(b) Our Model

Figure 2: ARTEMIS spacecraft shape models.

The ARTEMIS spacecraft is spin-stabilized with its body-fixed frame spin-axis pointed towards the south celestial pole. The attitude of the spacecraft was frequently estimated during the mission and was generally kept to within a few degrees of the south celestial pole [19, 20]. A time history of the spacecraft’s attitude has been implemented in our simulations in order to determine the area necessary for SRP calculations.

Throughout the mission, station-keeping maneuvers and small attitude burns were executed. Station-keeping maneuvers were generally on the order of less than a m/s in total imparted delta-V [21, 22]. It was assumed that the attitude burns that were executed were small and on the order of a mm/s or less. A time history of both station-keeping maneuvers and small attitude burns were also implemented in this analysis. While sufficient details for the station-keeping maneuvers (execution time and designed delta-V) are known, only the attitude maneuver execution time is known. Therefore, all initial estimates of these maneuvers are set to be 0.0 mm/s.

Once all of the models necessary to represent the mission were implemented, the orbit determination filter was initialized. In this work, a multitude of parameters are estimated. In general, every navigation solution estimated the spacecraft’s position and velocity, an SRP scale factor, stochastic

Table 1: Orbit determination filter uncertainties.

| Estimation Parameters | <i>a priori</i> uncertainty (1-sigma) |
|--------------------------------------|--|
| Spacecraft position | 100 km |
| Spacecraft velocity | 1 m/s |
| SRP Coefficient | 10% |
| Spacecraft Reflectivity Coefficients | |
| Specular | 0.1 |
| Diffuse | 0.1 |
| Empirical Accelerations | |
| Radial | 5e-12 km/s ² |
| Transverse | 5e-12 km/s ² |
| Normal | 5e-12 km/s ² |
| Station Keeping Maneuvers | |
| X, Y, Z | 10.0 mm/s |
| Start Time | 10.0 s |
| Attitude Maneuvers | |
| X, Y, Z | 1.0 mm/s |
| Start Time | 10.0 s |
| DSN per-pass range bias | 5 m |
| DSN measurements | |
| Range | 2 m |
| Doppler | 0.1 mm/s |
| Berkeley measurements | |
| Range | N/A |
| Doppler | 2 mm/s |
| Consider Parameters | |
| Media Calibrations | |
| Earth Orientation Parameters | |
| DSN Station Locations | |

accelerations, station-keeping maneuvers, attitude maneuvers, and per-pass range biases. In certain cases, the specular and diffuse coefficients of the cylindrical bus, top plate, and bottom plate of the spacecraft model were estimated. Every navigation solution had errors in media calibrations (tropospheric and ionospheric delays), EOPs, and station locations as considered states. A list of the *a priori* uncertainties for the estimated and consider parameters, as well as observables, is given in Tab. 1. The measurement weighting was updated with the standard deviation of the postfit residuals after each filter iteration until convergence. For the cases presented in this work, 10 iterations of the filter were performed.

3. Overview of Initial Results

Given the approaches and spacecraft parameters discussed in the previous section, initial results processing the raw tracking data were generated for short arcs of less than 7 days commensurate with that performed by the operations team. The time period under examination begins on November

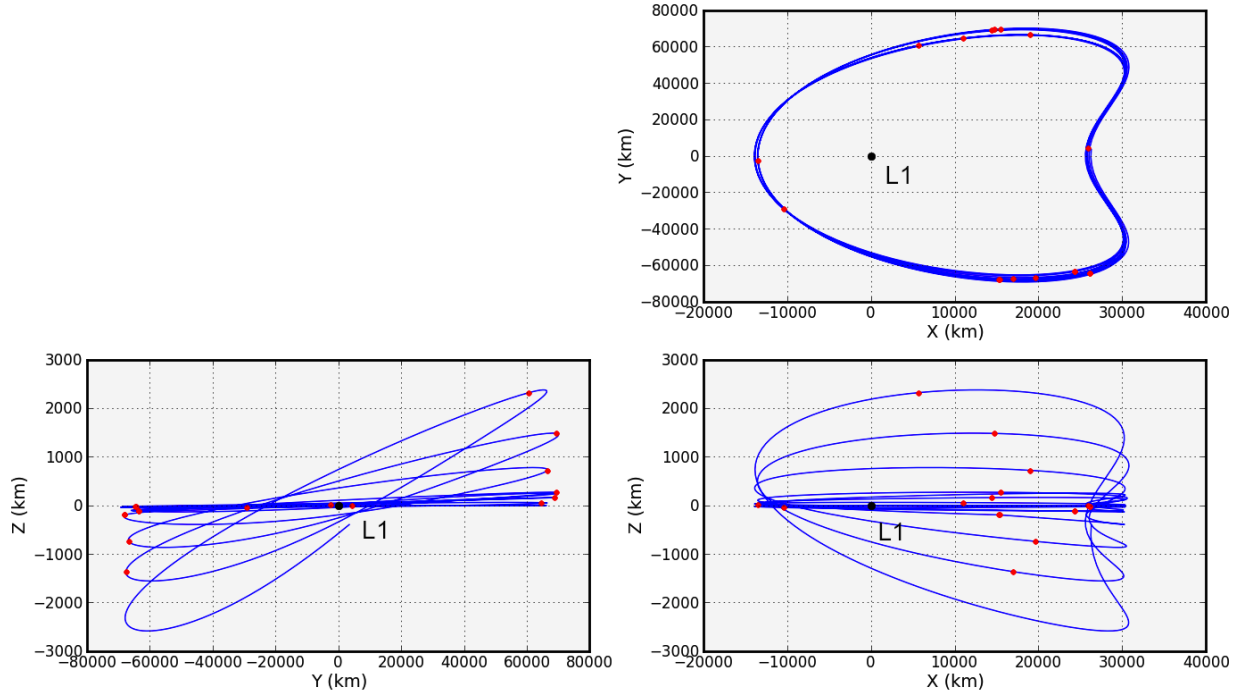


Figure 3: ARTEMIS-P2 trajectory from 19-NOV-2010 to 13-MAR-2011 displayed in the Earth-Moon rotating frame (Earth is in the -X axis with the Moon in the +X axis). The red dots represent the locations of Station Keeping Maneuvers that were performed during the mission.

19, 2010 and goes until March 14, 2011. Fig. 3 shows the ARTEMIS-P2 trajectory that was under evaluation in this work. This period was chosen for analysis due to the fact that there was relatively low solar activity during this time-frame. The initial goal of this analysis was to obtain a detailed estimate of the spacecraft SRP parameters for use in later analyses.

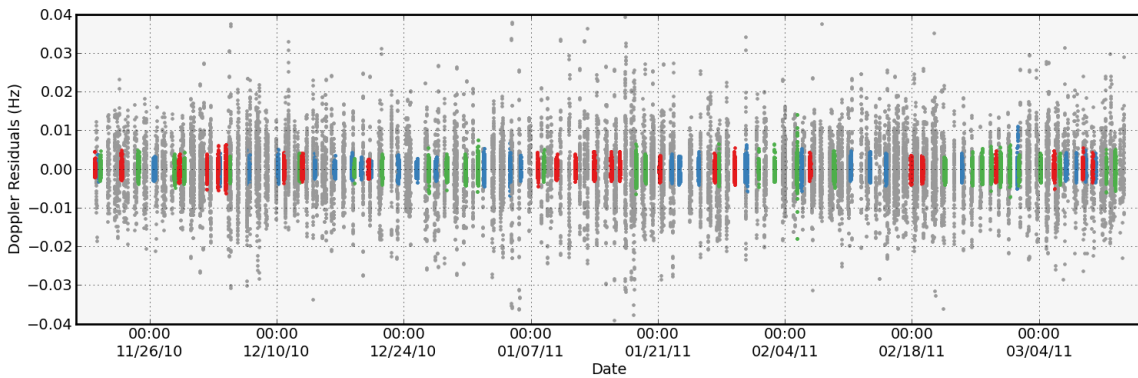


Figure 4: Doppler post-fit residuals for entire timeframe under analysis for Goldstone (blue), Canberra (green), Madrid (red), Berkeley (grey).

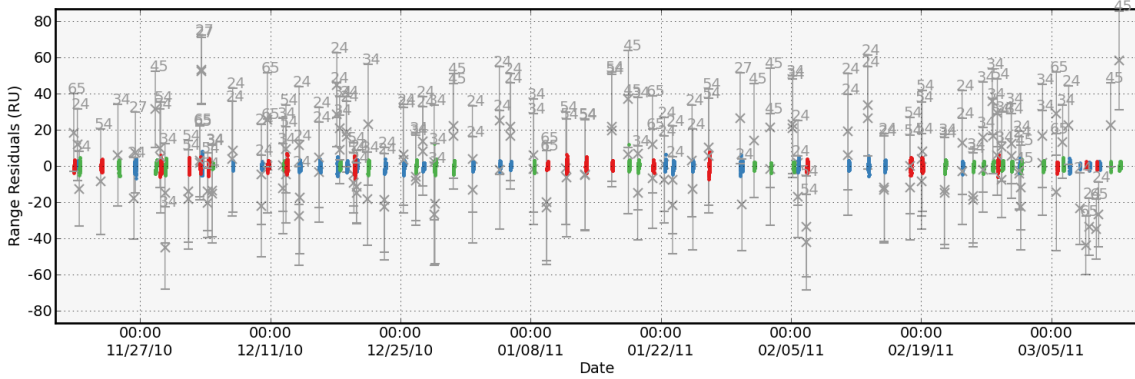


Figure 5: Range post-fit residuals with range biases for entire timeframe under analysis for Goldstone (blue), Canberra (green), Madrid (red), Berkeley (grey).

Both short 7-day arcs and long 14-day arcs were evaluated over the 4 month time period of concern. Initial results spanning this time frame estimated position, velocity, SRP scale factor, and stochastic accelerations. The post-fit Doppler residuals for the 4 month time-span from the 14-day arc solutions is shown in Fig. 4. For reference, 1 mm/s corresponds to approximately 15.3 mHz. As expected the Berkeley Doppler data was considerably noisier than the DSN Doppler data. In addition, the tracking arc duration for Berkeley was considerably less than the DSN. In all of the following filter solutions, the data was weighted according to their post-fit residual standard deviations. Fig. 5 shows the post-fit range residuals for the DSN stations with their estimated per-pass range biases. Range data was weighted at a minimum of 2 m for the following filter solutions with an initial per-pass range bias uncertainty of 5 m. For reference, approximately 7 range units (RU) is 1 m.

As a test to see if the post-fit residuals were Gaussian noise, a histogram of all post-fit residuals by station was examined. Fig. 6 shows the distribution of post-fit residuals for the Doppler measurements by station for the entire analysis period. On average, the Berkeley ground station (BRKS) had a Doppler residual of roughly 8 mHz with the DSN stations 1.8 mHz. While BRKS

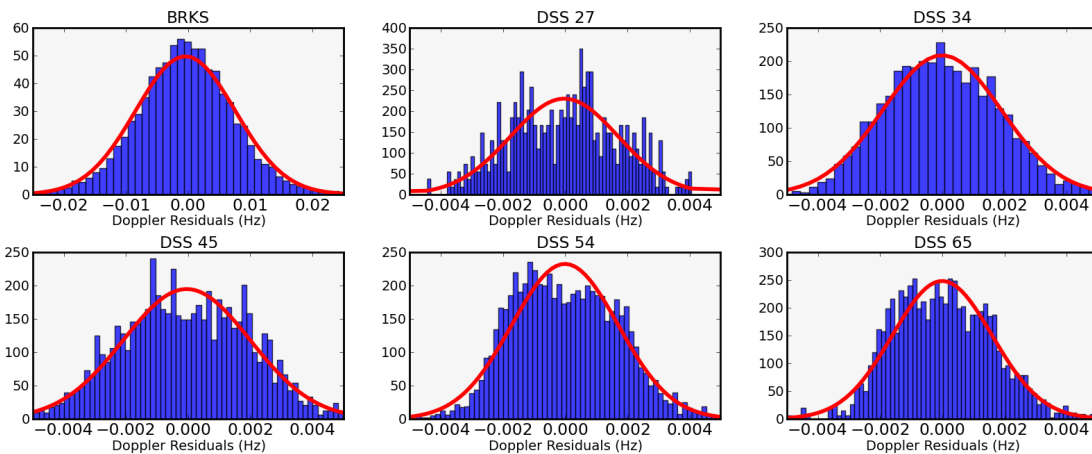
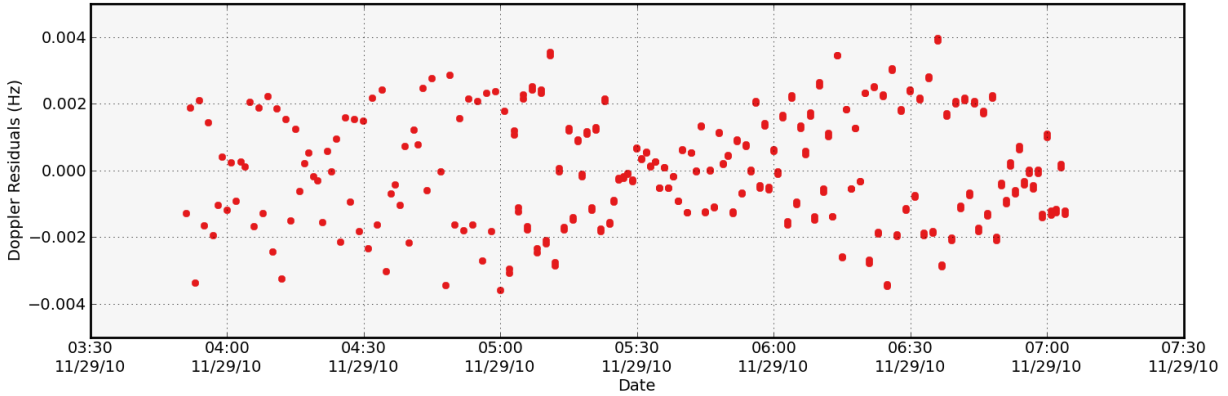
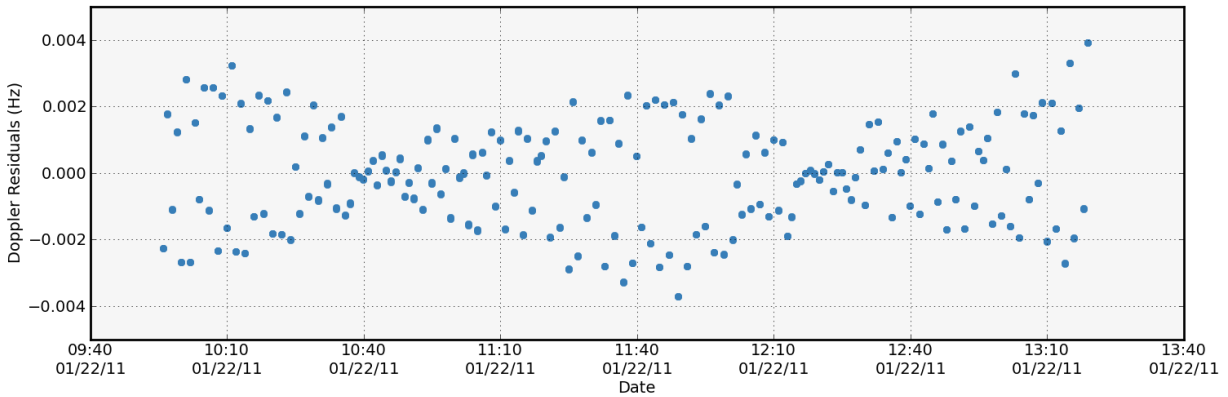


Figure 6: Histogram of Doppler residuals by station



(a) Spin signature seen in November



(b) Spin signature seen in January

Figure 7: Spin signature seen in Doppler residuals throughout the data arcs for 2 passes in different months.

seems Gaussian, the other DSN stations do not. Fig. 6 shows an increased prominence of Doppler residuals for the DSN ground stations. It was also noticed on certain passes that the residuals seemed to have a sometimes periodic or bounded structure at a few mHz. This periodic or bounded behavior in the post-fit Doppler residuals is persistent throughout the entire data arc.

After a quick FFT analysis of the 60 sec count Doppler data for a subset of data arcs, a periodic structure was noticeable. It was determined that this signature is most likely due to a slight offset between the spin axis and the antenna which resulted in a slight modulation in the Doppler data. Fig. 7 shows two DSN Doppler passes during the time period under analysis. Fig. 7(b) clearly has a defined structure to it due to the spin rate of the spacecraft. Since this is 60 sec count Doppler, the signal is significantly aliased. In certain cases, the Doppler residuals appeared to have slight precession and nutation as well. In order to confirm that this signature is due to the spinning spacecraft, an FFT analysis was performed on dense BRKS Doppler data. The dense BRKS Doppler data is given at sparse times throughout the beginning of the analysis period at a rate of 10Hz. The FFT resulted in a peak frequency that was identical to the spin rate determined from telemetry at that time. Even though the 10Hz BRKS Doppler data is incredibly noisy, a frequency can

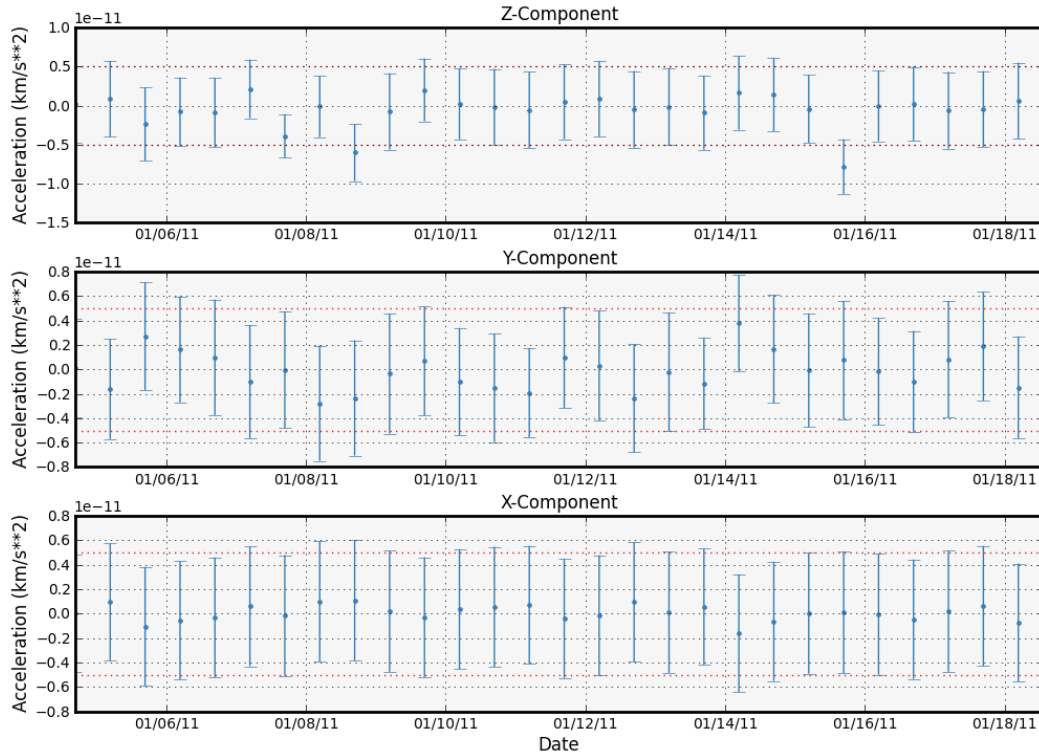


Figure 8: Example of stochastics fit during a Long Arc: Z-axis is S/C-Moon line

still be determined. The estimation of the spin state and removal of the spin signature from the Doppler measurements was not performed in this analysis. Instead, the DSN Doppler measurements were de-weighted accordingly. The periodic structure being noticeable at the 2 to 4 mHz level is commensurate with the expected uncertainty of the DSN Doppler data.

A benefit of using a sequential filter to estimate the spacecraft state is that the estimation of stochastic accelerations can be included. The process of adding stochastic accelerations to a batch estimator, although it can be done, is quite difficult. The idea behind stochastic acceleration estimation is to pick up any unmodeled perturbations that the dynamics are not accounting for. Ideally, one would like the stochastics to be zero mean with slight deviations throughout the trajectory. There are cases where certain parameters, like an increase in solar irradiance causing an increase SRP force, cannot be modeled. In these cases, stochastic acceleration estimation is desired. Fig. 8 shows the estimated white-noise stochastic accelerations over a 14 day data arc. Though there are slight variations in the stochastic accelerations, they remain close to zero.

4. Solar Coefficient Results

In an effort to increase the fidelity of the spacecraft model used in this analysis, specific focus was placed on estimating the spacecraft parameters that impact the effect of solar radiation pressure on the evolution of the trajectory. Gravitational perturbations are well defined and straightforward to implement with a high degree of fidelity. Solar perturbations on the other hand are susceptible to variations in spacecraft characteristics, attitude, and solar activity. A detailed model of the

Table 2: ARTEMIS SRP Specular Coefficient Change (NORMALIZED)

| | Bus Cylinder | Bus Top Plate | Bus Bottom Plate |
|----------------|--------------|---------------|------------------|
| Arc 1 | 0.9099 | N/A | 1.0337 |
| Arc 2 | 0.9449 | 0.9717 | 0.9663 |
| Arc 3 | 0.9704 | 0.9783 | N/A |
| Arc 4 | 1.0309 | 1.0057 | N/A |
| Arc 5 | 0.9575 | 1.0267 | N/A |
| Arc 6 | 1.0070 | 1.0364 | N/A |
| Arc 7 | 1.1793 | 0.9811 | N/A |
| Average | 1.0000 | 1.0000 | 1.0000 |

Table 3: ARTEMIS SRP Diffuse Coefficient Change (NORMALIZED)

| | Bus Cylinder | Bus Top Plate | Bus Bottom Plate |
|----------------|--------------|---------------|------------------|
| Arc 1 | 0.8576 | N/A | 1.0025 |
| Arc 2 | 0.8833 | 0.9993 | 0.9975 |
| Arc 3 | 0.9263 | 0.9982 | N/A |
| Arc 4 | 1.0591 | 1.0005 | N/A |
| Arc 5 | 0.9788 | 1.0074 | N/A |
| Arc 6 | 1.0499 | 1.0050 | N/A |
| Arc 7 | 1.2450 | 0.9895 | N/A |
| Average | 1.0000 | 1.0000 | 1.0000 |

spacecraft shape was used in the analysis presented in this paper. The model used is represented by the shape model shown in Fig. 2(b) in a previous section. In order to increase the fidelity of the spacecraft parameters that are effected by SRP, seven 14-day arcs were used to estimate the specular and diffuse coefficients for the spacecraft cylindrical bus, top plate, and bottom plat. The spacecraft shape and area parameters were kept constant throughout the filter runs. The attitude of the spacecraft shape model was updated regularly when attitude maneuvers were known to be performed. The filter solutions were iterated until there was very little change in the specular and diffuse coefficients. The purpose of this analysis was to determine an average solution to the spacecraft parameters for future use in data arcs. Tab. 2 gives the normalized values of the specular coefficients for the three spacecraft shapes being estimated. The values are normalized based on the average value of all seven data arcs. Tab. 3 gives the normalized values of the diffuse coefficients for the three spacecraft shapes being estimated. Out of all of the parameters being estimated, the diffuse coefficient for the bus cylinder was the most difficult to converge on. All of the other specular and diffuse coefficients settled onto nominal values.

5. Short-arc Overlaps

The overlap strategy that was used in this section was that of generating solutions using 5 days worth of tracking data immediately after a station keeping maneuver and compare this to solutions where the epoch began 5 days before the next station keeping maneuver. Nominally, this produced an overlap of about 3 days where the typical duration between station keeping maneuvers was a

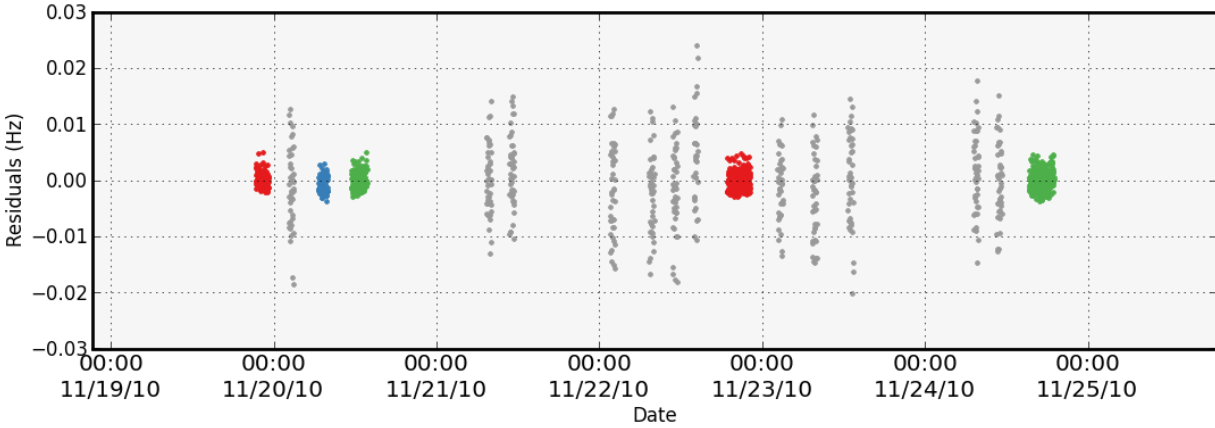


Figure 9: Short Arc Doppler tracking

week. A key consideration for these short-arc evaluations was whether the filter would be able to converge in enough time to perform meaningful comparisons between station-keeping maneuvers. The tracking data available is relatively sparse as shown in Fig. 9. Typically, 5 DSN passes were performed for each short-arc overlap analysis. The number of BRKS Doppler passes was usually 10 or more. Five days of tracking allowed for the initial position uncertainty to come down to 500 m or less in each coordinate with solutions converging after a few iterations.

Given these conditions, evaluation of the precision of the orbit solutions was possible during these short-arc periods. Fig. 10 and Fig. 11 demonstrate the precision as evidenced by short-arc overlap analyses described previously. Fig. 10 shows the position Radial, In-track, Cross-track, and 3D-RMS overlap precision for the short-arc analysis. The average short-arc overlap position errors are 15 ± 8 m Radial, 183 ± 146 m In-track, and 416 ± 247 m Cross-track. The average short-arc overlap velocity errors are 0.263 ± 0.182 mm/sec Radial, 1.427 ± 1.516 mm/sec In-track, and 2.825 ± 1.730 mm/sec Cross-track.

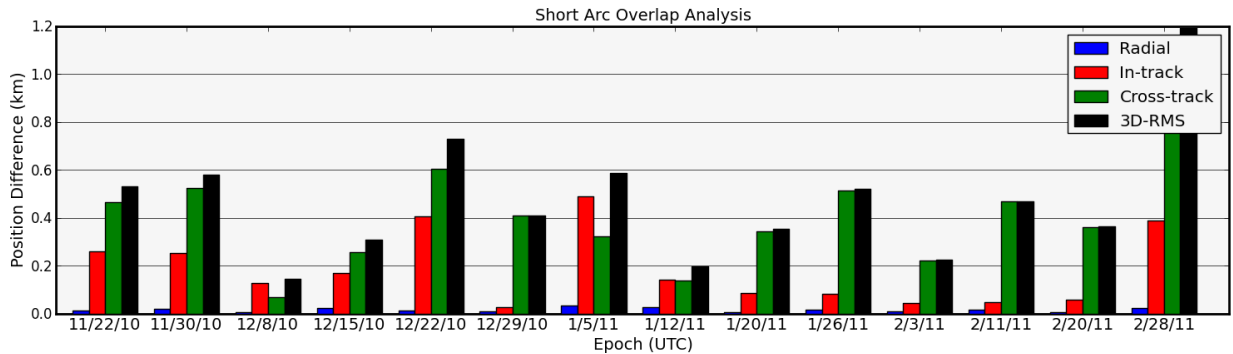


Figure 10: Short Arc Position Overlap Analysis

The evaluations in this section and the subsequent section were estimated with an initial state derived from the spacecraft ephemeris which was subsequently perturbed.

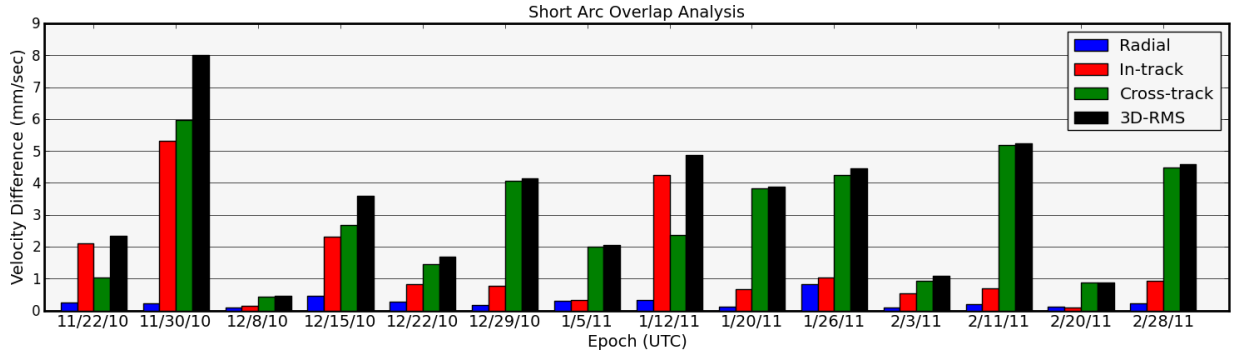


Figure 11: Short Arc Velocity Overlap Analysis

6. Long-arc Overlaps

The short-arc overlap analysis contained data arcs and filter solutions that did not go over maneuvers and thus did not estimate station keeping maneuvers. The overlap strategy used in this section was to start a data arc just after a station keeping maneuver and estimate over a single station keeping maneuver with the data cut off just prior to the next station keeping maneuver. A second overlap was initialized just after the estimated station keeping maneuver in the preceding data arc and continued over the next maneuver ending just prior another maneuver. This left about a 7 day overlap to compare the two solutions which generally spanned 14 days. There was significantly more tracking data during the long arcs than the short arcs. Fig. 12 and Fig. 13 demonstrate the precision as evidenced by long-arc overlap analyses described previously. Fig. 12 shows the position Radial, In-track, Cross-track, and 3D-RMS overlap precision for the short-arc analysis. The average long-arc overlap position errors are 5 ± 4 m Radial, 66 ± 50 m In-track, and 102 ± 53 m Cross-track. The average long-arc overlap velocity errors are 0.062 ± 0.048 mm/sec Radial, 0.283 ± 0.221 mm/sec In-track, and 0.687 ± 0.048 mm/sec Cross-track.

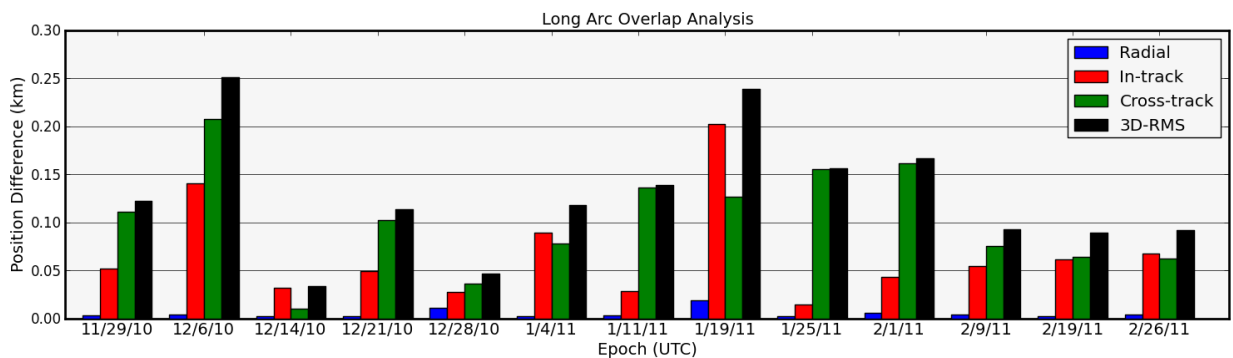


Figure 12: Long Arc Position Overlap Analysis

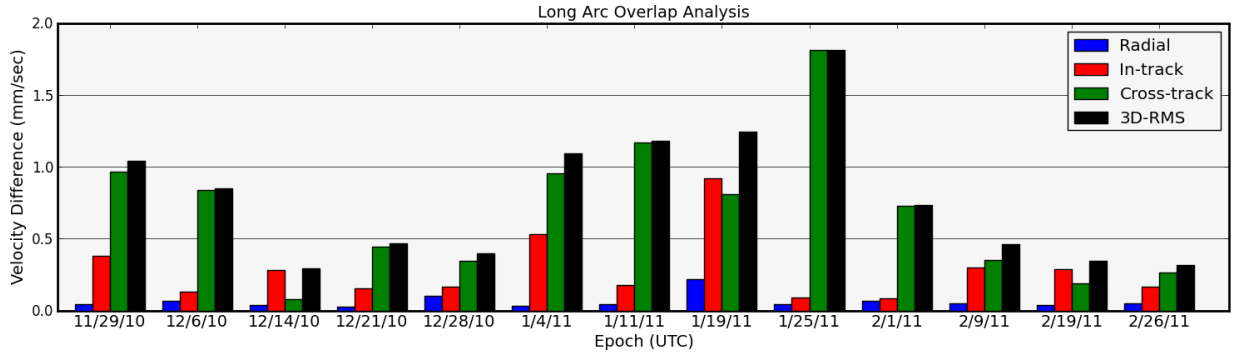


Figure 13: Long Arc Velocity Overlap Analysis

7. Solutions Considering Maneuvers

As noted in the previous section, the sequential filter set-up enabled for solutions to span station-keeping maneuvers. In solving for filter runs that span maneuvers, the filter is able to obtain an estimate of the maneuver. The results discussed in this section were estimated from the filter given an *a priori* estimate of the timing of the maneuvers and no *a priori* information about the magnitude or direction of the maneuvers.

For this evaluation, 17 station-keeping maneuvers were estimated spanning a time frame from November 2010 and March 2011 for the P2 spacecraft. The estimated maneuvers were compared to the maneuvers designed by the mission team at Goddard Space Flight Center. These designed maneuvers do not include variations in the maneuver magnitude or direction caused by translation of the original design, done in AGI Satellite Tool Kit, into the maneuver commands constrained by the spacecraft performance constraints. The data used to generate the comparisons shown in Tab. 4 were derived by comparing the magnitude and the directional components of the maneuvers as designed and as estimated. The directional components are defined in the True of Date reference frame. The level of fidelity in the estimated solution as a result of the improved solar coefficients and the long data arcs enabled this evaluation.

Table 4: Maneuver Evaluation (Designed-Estimated)

| | Mag. (mm/s) | Mag. (%) | X (mm/s) | X (%) | Y (mm/s) | Y (%) | Z (mm/s) | Z (%) |
|---------|-------------|----------|----------|-------|----------|-------|----------|--------|
| Average | 1.98 | 1.49 | 0.93 | 1.78 | 3.39 | 9.43 | 2.94 | 48.23 |
| Median | 0.71 | 0.58 | 0.61 | 1.10 | 1.98 | 5.69 | 1.78 | 6.51 |
| Max | 19.0 | 7.28 | 3.78 | 6.98 | 20.7 | 31.86 | 12.7 | 451.03 |
| Min | 0.10 | 0.03 | 0.21 | 0.06 | 0.06 | 0.30 | 0.25 | 1.22 |

Using a different method that leveraged differences in spacecraft state from propagated solutions, Woodard et al. performed a similar evaluation and obtained results of similar magnitude.[23] This data shows that, in general, the the magnitude and x-component of the maneuvers were accurately executed and estimated whereas the y-components and z-components were seen have larger variations between what was estimated and what was designed.

8. Summary and Future Work

The work completed to date has demonstrated an ability to post-process raw tracking data from the ARTEMIS mission during the LPO phase of the mission. The navigation solutions generated are able to resolve spacecraft spin signatures which suggests the filter is fitting the Doppler data well. Analysis was performed to obtain accurate solar radiation pressure estimates for the P2 spacecraft which was subsequently used in the analysis and was shown to be relatively consistent over the arcs evaluated. Overlap analyses demonstrated precision of the orbit solution to be 128 ± 62 m for position 3D-RMS and 0.788 ± 0.448 mm/s for velocity 3D-RMS. The ability to filter over and subsequently estimate maneuvers was leveraged to compare designed and estimated station-keeping maneuver solutions. These differences were observed to be small, as a percentage of the total maneuver, in magnitude and the True of Date x-components of the maneuvers. The True of Date y-components and z-components were observed to have higher variations which could be caused by poor maneuver performance in those directions or poor observability of those directions within the navigation solutions.

During this work it was observed that the attitude maneuvers performed by the spacecraft had a noticeable impact on the solution fit and precision. Preliminary results suggest that this impact is on the order of hundreds of meters in position when comparing solutions with and without these attitude maneuvers modeled. Future work will evaluate this initial observation.

Additional future work will investigate the overall data-set including evaluation with respect to attitude maneuvers, investigation of additional arcs of data, identification of filter or model parameters that yield improved solutions in terms of lower uncertainty and higher precision. This work will seek to systematically identify unmodeled accelerations observed in the stochastics of the solutions present here. This identification has the potential to increase the fidelity of the dynamics and thus increase the accuracy and convergence speed of future solutions. Future analysis will also evaluate data from the P1 spacecraft. This additional data-set is expected to provide valuable insight on the effect of spacecraft parameters on the navigation solution since both spacecraft are identical.

Overall the objective of future work is to improve the body of knowledge accessible for mission designers and spacecraft navigators of future missions within the Earth-Moon three-body regime.

9. Acknowledgments

This work was supported by a NASA Space Technology Research Fellowship.

This material is based upon work supported by the National Science Foundation Graduate Research Fellowship under Grant No. DGE 1144083.

We acknowledge NASA contract NAS5-02099 and V. Angelopoulos for use of data from the THEMIS Mission. Specifically: M. Bester and D. Cosgrove for the use of spacecraft tracking data.

We acknowledge Caltech and the Jet Propulsion Laboratory for use of MONTE software.

This work would not have been possible without the support of David Folta and Mark Woodard at NASA Goddard Space Flight Center who provided valuable input into the operations and planning conducted during the period of interest during the ARTEMIS mission.

Valuable contributions to this work were made by the following graduate students within the Colorado Center for Astrodynamics Research: Stephen Phillips contributed to the code required to read and utilize raw tracking data, Nicholas Ravago contributed to the code and procedures required for processing tropospheric and ionospheric corrections, and Ben Bradley contributed to the code used for processing ionospheric data.

10. References

- [1] Hill, K., Parker, J. S., Born, G. H., and Demandante, N. “A Lunar L2 Navigation, Communication, and Gravity Mission.” “AIAA/AAS Astrodynamics Specialist Conference,” AIAA 2006-6662. AIAA/AAS, Keystone, Colorado, August 2006.
- [2] Folta, D. and Vaughn, F. “A Survey of Earth-Moon Libration Orbits: Stationkeeping Strategies and Intra-Orbit Transfers.” “AIAA/AAS Astrodynamics Specialist Conference and Exhibit,” AIAA 2004-4741. AIAA/AAS, Providence, Rhode Island, August 16–19, 2004.
- [3] Woodard, M., Folta, D., and Woodfork, D. “ARTEMIS: the first mission to the lunar libration orbits.” “21st International Symposium on Space Flight Dynamics. Centre National d’Études Spatiales, Toulouse, France,” 2009.
- [4] Broschart, S. B., Chung, M. J., Hatch, S. J., Ma, J. H., Sweetser, T. H., Weinstein-Weiss, S. S., and Angelopoulos, V. “Preliminary Trajectory Design for the ARTEMIS Lunar Mission.” A. V. Rao, T. A. Lovell, F. K. Chan, and L. A. Cangahuala, editors, “Proceedings of the AAS/AIAA Astrodynamics Specialist Conference held 9-13 August 2009, Pittsburgh, Pennsylvania,” Vol. 134 of *Advances in Astronautical Sciences*. AAS/AIAA, Univelt Inc., San Diego, CA, 2009.
- [5] Angelopoulos, V. “The ARTEMIS mission.” *Space science reviews*, Vol. 165, No. 1-4, pp. 3–25, 2011.
- [6] Cheetham, B. W. and Born, G. H. “Evaluating Orbit Determination Post-Processing Methods for Operational Artemis Data.” “AAS/AIAA Astrodynamics Specialist Conference held August,” 2011.
- [7] Sunseri, R. F., Wu, H.-C., Evans, S. E., Evans, J. R., Drain, T. R., and Guevara, M. M. “Mission Analysis, Operations, and Navigation Toolkit Environment (Monte) Version 040.” “NASA Tech Briefs,” Vol. 45. September 2012.
- [8] Bierman, G. *Factorization methods for discrete sequential estimation*, Vol. 128. Academic Press, 1977.
- [9] Tapley, B., Schutz, B., and Born, G. *Statistical Orbit Determination*. Academic Press, 2004.
- [10] Sabol, C. A. *A role for Improved Angular Observations in Geosynchronous Orbit Determination*. Ph.D. thesis, University of Colorado, Boulder, Colorado, 1998.

- [11] Sibois, A. E. GPS-based Sub-Hourly Polar Motion Estimates: Strategies and Applications. Ph.D. thesis, University of Colorado Boulder, 2011.
- [12] Niell, A. E. “Global mapping functions for the atmosphere delay at radio wavelengths.” *Journal of Geophysical Research: Solid Earth* (1978–2012), Vol. 101, No. B1, pp. 3227–3246, 1996.
- [13] Estefan, J. and Sovers, O. “A comparative survey of current and proposed tropospheric refraction-delay models for DSN radio metric data calibration.” *Jet Propulsion Lab. Report*, Vol. 1, 1994.
- [14] Petit, G. and Luzum, B. “IERS conventions (2010).” Tech. rep., DTIC Document, 2010.
- [15] Schaer, S., Gurtner, W., and Feltens, J. “IONEX: The ionosphere map exchange format version 1.” “*Proceedings of the IGS AC Workshop, Darmstadt, Germany,*” Vol. 9. 1998.
- [16] Folkner, W. M., Williams, J. G., and Boggs, D. H. “The Planetary and Lunar Ephemeris DE 421.” Tech. Rep. IOM 343R–08–003, Jet Propulsion Laboratory, California Institute of Technology, March 2008. ftp://naif.jpl.nasa.gov/pub/naif/generic_kernels/spk/planets/de421_announcement.pdf.
- [17] Tapley, B., Ries, J., Bettadpur, S., Chambers, D., Cheng, M., Condi, F., Gunter, B., Kang, Z., Nagel, P., Pastor, R., Pekker, T., Poole, S., and Wang, F. “GGM02 - An Improved Earth Gravity Field Model from GRACE.” *Journal of Geodesy*, Vol. 79, No. 8, pp. 467–478, 2005.
- [18] Konopliv, A. S., Park, R. S., Yuan, D., Asmar, S. W., Watkins, M. M., Williams, J. G., Fahnestock, E., Kruizinga, G., Paik, M., Strelakov, D., et al. “The JPL lunar gravity field to spherical harmonic degree 660 from the GRAIL Primary Mission.” *Journal of Geophysical Research: Planets*, Vol. 118, No. 7, pp. 1415–1434, 2013.
- [19] Markley, F. L. and Sedlak, J. E. “Kalman filter for spinning spacecraft attitude estimation.” *Journal of guidance, control, and dynamics*, Vol. 31, No. 6, pp. 1750–1760, 2008.
- [20] Hashmall, J. A., Felikson, D., and Sedlak, J. E. “Use of Fuzzycones for Sun-Only Attitude Determination: THEMIS Becomes ARTEMIS.” “*21st International Symposium on Spaceflight Dynamics, Toulouse,*” 2009.
- [21] Marchese, J. E., Owens, B. D., Cosgrove, D., Frey, S., and Bester, M. “Calibration of In-flight Maneuver Performance for the THEMIS and ARTEMIS Mission Spacecraft.” “*Proceedings of the AIAA 2010 SpaceOps Conference,*” pp. 25–30. 2010.
- [22] Owens, B. D., Marchese, J. E., Cosgrove, D. P., Frey, S., and Bester, M. G. “Optimizing ARTEMIS Libration Point Orbit Stationkeeping Costs Through Maneuver Performance Calibration.” “*Proceedings of the 22nd AAS/AIAA Space Flight Mechanics Meeting,*” 2012.
- [23] Woodard, M., Cosgrove, D., Morinelli, P., Marchese, J., Owens, B., and Folta, D. “Orbit Determination Of Spacecraft In Earth-Moon L1 And L2 Libration Point Orbits.” “*Proceedings of the 2011 AAS/AIAA Astrodynamics Specialists Conference,*” AAS 11–514, July 31 – August 4, 2011, Girdwood, Alaska 2011.